Vol. 87 (1995) *ACTA PHYSICA POLONICA A* No. 1

Proceedings of the XXIII International School of Semiconducting Compounds, Jaszowiec 1994

DILUTED MAGNETIC SEMICONDUCTORS IN HIGH MAGNETIC FIELDS

Y. SHAPIRA

Department of Physics, Tufts University, Medford MA 02155, USA
and
GES, Université Montpellier II
Place E. Bataillon, 34095 Montpellier Cédex 5, France

Magnetization studies of diluted magnetic semiconductors in high fields are reviewed. Magnetization steps due to pairs were originally used to measure the near neighbor exchange constant J_1. They are now also used to determine: (1) the smaller exchange constants J_2 and J_3, (2) the difference between J_1's for inequivalent near neighbors in wurtzite diluted magnetic semiconductors, and (3) the Dzyaloshinski–Moriya interaction. A different type of magnetization step, due to isolated ions, is used to determine the uniaxial anisotropy of Co^{++} ions in wurtzite diluted magnetic semiconductors. In Fe-based diluted magnetic semiconductors the high-field magnetization exhibits two effects: (1) strong dependence on field direction in cubic diluted magnetic semiconductors, and (2) reversal of the uniaxial magnetization-anisotropy in wurtzite diluted magnetic semiconductors. In (100) EuTe/PbTe superlattices the antiferromagnetic transition, both at zero and finite H, is depressed when the EuTe layer becomes only a few monolayers thick. The easy directions are in the (100) plane of the layer, which is explained by the dipole–dipole anisotropy.

PACS numbers: 75.50.Pp, 75.30.Et, 75.70.Fr

1. Introduction and scope

Many laboratories are equipped with 9 T superconducting magnets. Much higher magnetic fields are available only in a few installations. At present the maximum available dc fields are near 30 T. Experiments in higher fields are performed in pulsed magnets. Non-destructive pulsed fields of ≈ 60 T (with the sample surviving) have been produced, but 45 T pulsed fields are more common.

Any diluted magnetic semiconductor (DMS) can be viewed as being composed of two subsystems: magnetic and electronic. The magnetic subsystem consists of the $3d$ (or $4f$) magnetic ions. The electronic subsystem consists of the s-like electrons and p-like holes near the band edges. The unique properties of DMS arise

from the *sp–d* interaction which couples the two subsystems. It leads to spectacular magneto-optical and magneto-transport effects [1, 2]. The magnetic subsystem itself, however, is also of great interest because DMS are excellent examples of dilute magnetic materials.

This talk focuses on high-field magnetization measurements in which we have been involved. Some similar measurements by other groups, and a few results below 9 T, are also included. All these studies relate only to the magnetic subsystem. Obviously, only a fraction of high-field research on DMS is reviewed here. Optical and transport studies, crucial for studying the effects of the *sp–d* interaction, are not included.

2. Magnetic ions and their interactions

Much of the DMS research to date has focused on II–VI compounds. Among these, Mn-based DMS have been studied most extensively, but Fe-based and Co-based DMS have also been investigated. There is now a strong evidence that the magnetic ions in these systems enter substitutionally into the cation sites, and are randomly distributed over these sites [3]. Random distribution means that the fact that a given cation site is occupied by a magnetic ion does not change the probability of occupancy of any nearby cation site. Thus, the probability that any cation site is occupied is equal to the fraction x of cations which are magnetic. The fact that the distribution of magnetic ions is random is very important. Had the magnetic ions tended to cluster (or avoid each other), any property would have depended on the degree of clustering, i.e., difficult to calculate from first principles.

Consider first the magnetic ions. The Mn^{++} and Co^{++} ions both contain an odd number of $3d$ electrons. Kramers theorem then implies that the ground level, at zero field, is degenerate. This level will undergo a Zeeman splitting in a field $\boldsymbol{H}$, leading to conventional type (Brillouin type) magnetism. In contrast, Fe^{++} has an even number of $3d$ electrons (six), leading to a singlet ground state. As a result, the magnetism of Fe^{++} is of the Van Vleck type, not of the Brillouin type [4].

The magnetism of Fe-based DMS is strongly dependent on crystal field parameters, and on the spin–orbit coupling constant λ, which control the energy-level structure of isolated Fe^{++} ions. Values for these parameters can be obtained from independent optical, IR, and Raman experiments. Exchange interactions between Fe^{++} ions are also important.

The Mn^{++} ion, in Mn-based DMS, is an S-state ion which acts as an ideal spin with $S = 5/2$ and $g = 2.0$. The crystal field splittings are very small, much less than 0.1 K [5]. In Co-based DMS the Co^{++} ion acts as a spin $S = 3/2$, but the g factor is about 2.3, instead of the pure-spin value 2.0 [6]. When the crystal structure is wurtzite (hexagonal symmetry) the Co^{++} ion is subjected to an axial crystal field, creating a single-ion anisotropy of the form DS_z^2. This anisotropy splits the 4-fold degenerate level ($S = 3/2$) into two doublets: $S_z = \pm 3/2$ on top and $S_z = \pm 1/2$ below. For Co^{++} in CdS or CdSe the separation $2D$ between the doublets is of order 1 K.

The dominant interaction between magnetic ions is the *d–d* exchange inter-

action. For spins i and j it has the form

$$\mathcal{H}_{\text{exch}} = -2J_{ij}\boldsymbol{S}_i \cdot \boldsymbol{S}_j. \tag{1}$$

The exchange constants J_{ij} in II–VI DMS are antiferromagnetic (negative, in our notation), and they decrease rapidly with the distance r_{ij}. The nearest-neighbor (NN) exchange constant J_1, which is the largest, is an order of magnitude larger than J_2 for next-nearest-neighbors (NNNs). The theory of the exchange interactions in Mn-based DMS is reviewed in [7].

Among the other interactions between the magnetic ions the most important is the Dzyaloshinski–Moriya (DM) interaction, of the form

$$\mathcal{H}_{\text{DM}} = -2\boldsymbol{D}_{ij} \cdot \boldsymbol{S}_i \times \boldsymbol{S}_j. \tag{2}$$

The largest D_{ij} is expected to be D_1. Its magnitude for Mn-based DMS was calculated by Larson and Ehrenreich [8]. They found that it increases with the atomic number of the *anion*. Even for the tellurides, for which D_1 is largest, the value of $|D_1/J_1|$ is only 0.05.

3. Magnetization steps

The leading techniques for measuring the largest exchange constant, J_1, use either high-field magnetization steps (MSTs) [3, 9] or inelastic neutron scattering [10]. The first generation of MSTs succeeded in determining J_1 in virtually all Mn-based II–VI DMS. More recently the technique has been extended along several lines: (1) the determination of J_1 in some Co-based II–VI DMS (CdCoS and CdCoSe) using 60 T pulsed fields [11]; (2) studies of inequivalent NNs in the wurtzite structure [12]; (3) determination of the smaller exchange constants J_2 and J_3 [13], and (4) observations of another type of MST, arising from isolated Co^{++} ions in wurtzite DMS [14].

Below, we start from a simple model which brings out the physics of the MSTs. We then discuss some of the newer developments.

3.1. The J_1 model

We assume that the magnetic ions are either Mn^{++} or Co^{++}, i.e., degenerate ground level at $H = 0$. The dominant exchange constant is J_1. In the J_1 model it is assumed that there are no other exchange interactions, or any other interactions except with the magnetic field $\boldsymbol{H}$.

For low x it is convenient to consider each magnetic ion as belonging to a particular type of "cluster". The smallest cluster is a "single", with no magnetic NNs. The next type of cluster is a "pair", i.e., two magnetic ions which are NNs of each other but which have no other magnetic NNs. Next in size are triplets (there are two types, open and closed), followed by quartets, quintets, etc.

Assuming a random distribution, one can calculate the probabilities for a magnetic ion to be in each type of cluster. For x up to several percent the largest probability is to be a single, and the next largest is to be in a pair. The main features of the magnetization curve for low x can then be recovered by considered only singles and pairs. In this approximation (which serves as a good beginning)

the magnetization is the sum of the magnetizations of singles and of pairs. The magnetization of singles follows the Brillouin function. At liquid helium temperatures it is nearly saturated at 10 T. The magnetization of pairs is much more interesting.

The energy levels of a pair at $H = 0$ are given by

$$E = -J_1[S_T(S_T + 1) - 2S(S + 1)], \tag{3}$$

where S_T is the total spin of the pair, and S is the spin of each of the ions (e.g., 3/2 for Co^{++}). The energy E is governed by S_T. The ground state has $S_T = 0$, corresponding to antiparallel spins. The next level is $2|J_1|$ higher, with $S_T = 1$. The highest level is with $S_T = 2S$, corresponding to parallel spins. The level structure at H = 0 is shown in Fig. 1a.

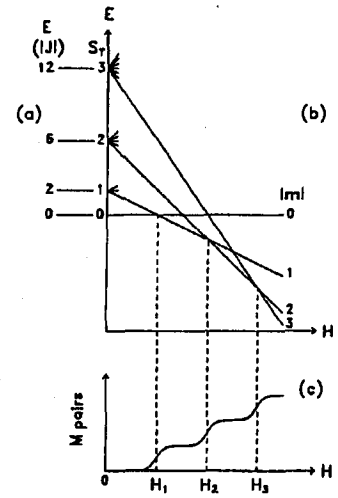

Fig. 1. (a) Energy level diagram for a pair of Co^{++} spins at $H = 0$. (b) Zeeman splitting of these levels. (c) Magnetization steps.

A magnetic field $\boldsymbol{H}$ splits all levels with $S_T > 0$, as shown in Fig. 1b. In this figure, m is the component of $\boldsymbol{S}_T$ along $\boldsymbol{H}$. The crucial point is that there are level crossings which change the ground state. Below H_1 the ground state has $m = S_T = 0$, but just above H_1 the ground state has a spin component $|m| = 1$ along $\boldsymbol{H}$. Just above H_2 the ground state has $|m| = 2$, etc.

At low T ($k_B T \ll 2|J_1|$) the changes in the value of m for the ground state lead to the magnetization steps shown in Fig. 1c. We shall refer to these MSTs as J_1 steps because they arise from J_1 pairs, each consisting of two spins coupled by J_1. The J_1 steps occur at the fields H_n ($n = 1, 2, \ldots 2S$) which, one can easily show, are given by

$$g\mu_B H_n = 2|J_1|n, \tag{4}$$

where g is the g-factor for the magnetic ion, and μ_B is the Bohr magneton.

Two pieces of information can be obtained from the J_1 steps: the value of J_1, and the concentration of J_1 pairs. In the J_1 model the value of J_1 is obtained

from H_n via Eq. (4). To obtain a more accurate value it is necessary to modify the model to include the weaker exchange interactions (J_2, J_3, etc.). These weaker interactions change Eq. (4) to

$$g\mu_B H_n = 2|J_1|n + \Delta_n, \tag{5}$$

where the shifts Δ_n are small compared to $2|J_1|$. An approximate treatment [15] shows that Δ_n are nearly independent of n so that J_1 is obtained from the difference between different H_n, e.g.,

$$g\mu_B(H_2 - H_1) = 2|J_1|. \tag{6}$$

The values of J_1 in virtually all Mn-based II–VI DMS were obtained from J_1 steps [3, 9, 16]. For these materials a typical value of J_1/k_B is -10 K. Such a value implies that the first J_1 step occurs typically near 15 T (150 kG). For Co-based II–VI DMS the values of J_1 are much higher [10], so that very high fields are required to observe the J_1 steps. Only recently was the first J_1 step observed in CdCoS and in CdCoSe using 60 T pulsed fields [11].

The concentration of J_1 pairs is obtained from the magnetization rise ΔM associated with each J_1 step. Each pair in the sample contributes a rise of $g\mu_B$ to the magnetic moment, corresponding to $\Delta|m| = 1$. In all experiments in which ΔM was analyzed the number of pairs was in reasonable agreement with random distribution.

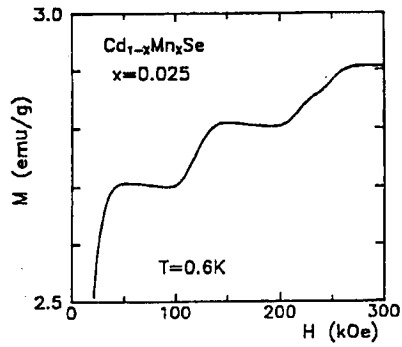

Fig. 2. The first two J_1 steps in CdMnSe. Note the structure in the second step [12].

Figure 2 shows an example of the first two magnetization steps in CdMnSe [12]. These data were taken in ^{3}He. An interesting feature is the structure observed in the second step, i.e., this step is composed of two "half-steps" of equal magnitude. We now discuss these half-steps.

3.2. Inequivalent NNs

The crystal structure of II–VI DMS is either zinc-blende (cubic) or wurtzite (hexagonal). In either structure there are 12 NN cation sites. In the zinc-blende structure all 12 possible NN pairs are equivalent by symmetry. In the wurtzite structure, however, there are two types of NN pairs. For one type, both magnetic

ions in the pair are in the same c plane. Among the 12 NN cations sites, 6 lead to such in-plane (or "in") J_1 pairs. The other 6 NN cations sites lead to J_1 pairs in which the two magnetic ions are not in the same c plane. These are the "out" J_1 pairs. Even in the ideal wurtzite structure, for which all 12 NN sites are equidistant (cation lattice is hcp), the "in" and "out" J_1 pairs are inequivalent by symmetry. In particular, the values of J_1 are slightly different. The reason is that although the dominant exchange path (through the intervening anion) is the same for all J_1 pairs, some of the other superexchange paths are not.

The difference between J_1^{in} and J_1^{out} splits each J_1 step into two half-steps of equal magnitude. The splitting (difference between the fields at the two half-steps) is proportional to n. Thus, the splitting of the second step is twice that of the first step, which explains why only the second step is split in Fig. 2. (The splitting of the first step was observed at much lower temperatures.)

Half-steps due to inequivalent NNs in the wurtzite structure were observed in CdMnS [17] and in CdMnSe [12]. In CdMnS the difference ΔJ_1 between the two J_1's is 13%. In CdMnSe it is 15%. A line-shape analysis for CdMnSe, which included the broadening of the MSTs caused by the DM interaction, showed that J_1^{in} is larger than J_1^{out}. The same analysis also gave an estimate for the DM constant D_1. All these results (magnitude and sign of ΔJ_1, and value of D_1) agree with theory [8, 18].

3.3. The J_1–J_2 model

In this model both J_1 and J_2 are included but all other exchange interactions are ignored [13]. Such a model presupposes that the second largest exchange constant is J_2, as expected, and that other exchange constants are much smaller. There are then four types of clusters: (1) singles, with no NNs or NNNs, (2) pure J_1 clusters (e.g., J_1 pairs with no NNNs), (3) pure J_2 clusters (e.g., J_2 pairs), and (4) mixed J_1–J_2 clusters (e.g., J_1 pairs for which one of the two spins also has a NNN).

In the context of the MSTs the most important effect of adding J_2 to the model is the appearance of a new series of MSTs, arising from J_2 pairs. These J_2 steps occur at fields H_n given by Eq. (5), but with J_1 replaced by J_2. Because J_2 is typically an order of magnitude smaller than J_1, the J_2 steps occur at much lower fields. This is shown in Fig. 3b. Adding J_2 to the model also leads to a fine structure in the J_1 steps, which is also shown in Fig. 3b. Often this fine structure is not resolved, so that it manifests itself as both a broadening of the J_1 steps and a small shift of H_n. (This shift is one of the contributions to Δ_n. The remaining contributions arise from J_3, J_4, etc.)

The most serious obstacle to observing J_2 steps is the temperature requirement $k_B T \ll 2|J_2|$. Thus far J_2 steps were observed only in Co-based DMS, in which the exchange interactions (including J_2) are relatively strong [13, 19].

There is, of course, no reason to stop at J_2. One can easily formulate a J_1–J_2–J_3 model. Such a model leads to J_3 steps, in addition to J_1 and J_2 steps. Both J_2 and J_3 steps were observed in ZnCoTe, which made it possible to test predictions for the distance dependence of J_{ij} [13].

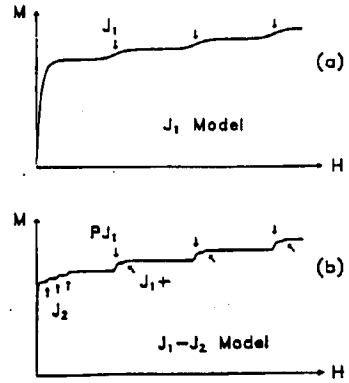

Fig. 3. (a) Magnetization curve, with J_1 steps, in the J_1 model. (b) Magnetization curve in J_1–J_2 model, showing the J_2 steps and the fine structure (PJ_1 and J_1+) in the J_1 steps [13].

3.4. Magnetization step due to singles

A completely different type of magnetization step occurs for isolated Co^{++} ions (singles) in the wurtzite structure. The energy level diagram for an isolated Co^{++} ion in this structure is shown in Fig. 4. The single-ion anisotropy DS_z^2 creates a zero-field splitting of magnitude $2D$, separating the $S_z = \pm 3/2$ doublet from the $S_z = \pm 1/2$ doublet.

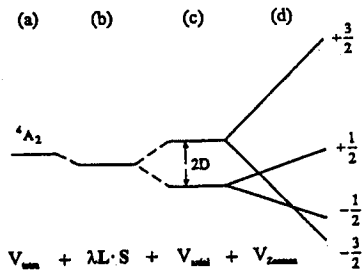

Fig. 4. Lowest energy levels of an isolated Co^{++} ion in CdS or CdSe, showing the effects of the tetrahedral field, the spin–orbit coupling, the axial anisotropy, and of a magnetic field $\boldsymbol{H}$ along the c axis.

At low temperatures, $k_BT \ll 2D$, the magnetization curve for $\boldsymbol{H} \parallel \boldsymbol{c}$ consists of two parts. First, the magnetization arising from the $\pm 1/2$ doublet follows a Brillouin function for $S = 1/2$, and becomes saturated. Then the $S_z = -3/2$ level crosses the $-1/2$ level, giving rise to a large magnetization step. This type of magnetization step is not new, but it is new in the context of DMS. It was observed in both CdCoS and CdCoSe [14]. Figure 5 shows some of the results.

In CdCoS the value of D obtained from the magnetization step for singles agreed with early EPR data, but in CdCoSe it did not. Recent EPR work in the

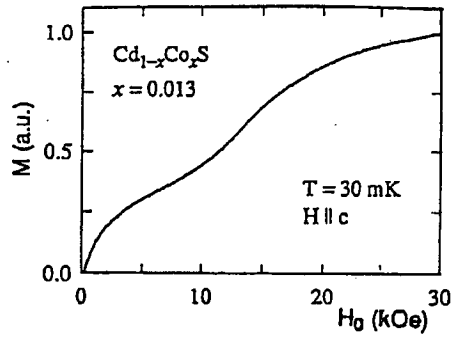

Fig. 5. Magnetization step arising from (nearly) isolated Co^{++} ions in CdCoS. These data were taken in a dilution refrigerator [14].

University of Montpellier and in the University of Zaragoza [20] showed that the value of D deduced from the early EPR work [21] was based on a misidentification of the resonance line observed at the higher field (5.7 kOe for $\boldsymbol{H} \parallel \boldsymbol{c}$). When this error is corrected, the EPR value for D agrees with that determined from the magnetization step.

4. Magnetization anisotropy for Fe^{++} ions

As noted, Fe^{++} has a singlet ground state which leads to Van Vleck type paramagnetism [4]. The magnetization of isolated Fe^{++} ions is then calculated using the crystal-field model, sometimes including also the Jahn–Teller effect.

Recent work on Fe-based II–VI DMS uncovered two interesting effects at high fields. First, in zinc-blende (cubic) DMS the high-field magnetization at low T is anisotropic [22–24]. It is largest for $\boldsymbol{H} \parallel [100]$, and smallest for $\boldsymbol{H} \parallel [111]$. This contrasts with the isotropic behavior at low fields. The dependence of the high-field magnetization on field direction decreases as T increases. For samples

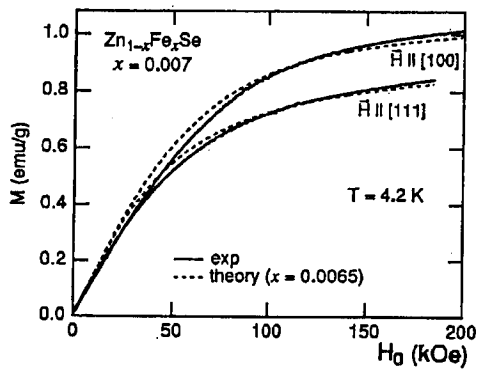

Fig. 6. Anisotropy of the magnetization of ZnFeSe at 4.2 K.

with low x (for which most magnetic ions are singles in the J_1 model) the effect is reasonably well described by the crystal-field model. Figure 6 compares some recent experimental results with theory [24].

A second effect was observed in wurtzite (hexagonal) materials, CdFeSe and CdFeS. At low H the magnetization for $\boldsymbol{H} \parallel \boldsymbol{c}$ is larger than for $\boldsymbol{H} \perp \boldsymbol{c}$, but above $\parallel$ 200 kOe the opposite is true [25, 26]. This reversal of the axial magnetization-anisotropy is expected from the crystal-field model.

5. EuTe/PbTe superlattices

EuTe has the rock salt structure (cubic symmetry). The Eu^{++} ions are S-state ions, each with spin 7/2, and they form a fcc lattice. Bulk EuTe orders antiferromagnetically at $T_N \approx 9.7$ K. The antiferromagnetic order is fcc type II, i.e., ferromagnetic (111) planes with the spins in adjacent planes pointing in opposite directions. The anisotropy is predominantly due to the dipole–dipole interaction, which makes the (111) planes the easy planes. If a high magnetic field is applied, it ultimately destroys the antiferromagnetic order at the "canted-to-paramagnetic" transition field H_c. For bulk EuTe at $T = 0$, $H_c = 72$ kOe [27].

Recently Kostyk et al. [28] investigated the magnetic properties of (100) EuTe/PbTe superlattices grown by MBE. The thickness of the EuTe layers varied from 1 to 8 atomic layers. The PbTe layers had a thickness of 30 atomic layers, designed to decouple the EuTe layers magnetically. A 2950 Å thick (100) EuTe film was also measured.

For the film the order–disorder phase transitions, both at T_N (zero field) and at H_c, were similar to those in the bulk. For the superlattice in which each EuTe layer consisted of 8 atomic layers the transitions were still similar to those in the bulk, but T_N and H_c were depressed by $\approx 10\%$. As the thickness decreased, the values of T_N and H_c became lower and the transitions broadened. For a monolayer of EuTe no transitions were found. These results are attributed to a loss of exchange bonds (near the surfaces) with decreasing thickness, and to a $3d \rightarrow 2d$ crossover of the lattice dimensionality.

At low fields ($H \ll H_c$) there are significant differences between the magnetizations for $\boldsymbol{H} \parallel [100]$ (normal to the layer) and $\boldsymbol{H} \parallel [010]$ (in the plane of the layer). For example, spin rotation (analogous to spin-flop) is seen for $\boldsymbol{H} \parallel [010]$ but not for $\boldsymbol{H} \parallel [100]$. These differences indicate that the spins at zero field are in the plane of the layer. Surprisingly, this result also holds for the 2950 Å film. Thus, the finite thickness of the (100) layer, or film, has a significant effect on the magnetic anisotropy.

In an early work on (111) EuTe/PbTe superlattices [29] the magnetic anisotropy (different from that observed by us) was attributed to strain associated with lattice mismatch. In contrast, we assumed that even in a superlattice the magnetic anisotropy of the EuTe layers was predominantly due to the dipole–dipole interaction. The reason is that the Eu^{++} is an S-state, so that its coupling to the lattice is very weak.

Calculations of the dipole–dipole anisotropy show that in (100) layers the easy axes are along the [011] and [0$\bar{1}$1] directions. These directions are at the

intersections of the (100) plane of the layer with the {111} planes, which are the easy planes in the bulk. The anisotropy which favors the special directions in the {111} planes is very nearly inversely proportional to the layer thickness. These results explain why the spins are observed to be in the (100) plane of the layer.

Acknowledgments

I am grateful to my many collaborators. This work was supported by NSF grant DMR-9219727 and by CNRS.

References

[1] *Semimagnetic Semiconductors and Diluted Magnetic Semiconductors*, Eds. M. Averous, M. Balkanski, Plenum, New York 1991.

[2] *Diluted Magnetic (Semimagnetic) Semiconductors*, Vol. 25 of *Semiconductors and Semimetals*, Eds. J.K. Furdyna, J. Kossut, Academic, New York 1988.

[3] Y. Shapira, *J. Appl. Phys.* **67**, 5090 (1990).

[4] A. Twardowski, *J. Appl. Phys.* **67**, 5108 (1990).

[5] For a review of EPR studies see S. Oseroff, P.H. Keesom, Ref. [2], and references therein.

[6] H.A. Weakliem, *J. Chem Phys.* **36**, 2117 (1962); M. Villeret, S. Rodriguez, R. Kartheuser, *Physica B* **162**, 89 (1990).

[7] B.E. Larson, H. Ehrenreich, *J. Appl. Phys.* **67**, 5084 (1990); K.C. Hass in Ref. [1].

[8] B.E. Larson, H. Ehrenreich, *Phys. Rev. B* **39**, 1747 (1989).

[9] Y. Shapira, in Ref. [1].

[10] T.M. Giebultowicz, J.J. Rhyne, J.K. Furdyna, P. Klosowski, *J. Appl. Phys.* **67**, 5096 (1990).

[11] S. Foner, private communication.

[12] V. Bindilatti, T.Q. Vu, Y. Shapira, C.C. Agosta, E.J. McNiff, Jr., R. Kershaw, K. Dwight, A. Wold, *Phys. Rev. B* **45**, 5328 (1992).

[13] T.Q. Vu, V. Bindilatti, Y. Shapira, E.J. McNiff Jr., C.C. Agosta, J. Papp, R. Kershaw, K. Dwight, A. Wold, *Phys. Rev. B* **46**, 11617 (1992).

[14] V. Bindilatti, N.F. Oliveira Jr., Y. Shapira, T.Q. Vu, D. Heiman, M. Demianiuk, *Solid State Commun.* **87**, 759 (1993), and to be published.

[15] B.E. Larson, K.C. Hass, R.L. Aggarwal, *Phys. Rev. B* **33**, 1789 (1986).

[16] R.R. Galazka, W. Dobrowolski, J.P. Lascaray, M. Nawrocki, A. Bruno, J.M. Broto, J.C. Ousset, *J. Magn. Magn. Mater.* **72**, 174 (1988).

[17] Y. Shapira, S. Foner, D. Heiman, P.A. Wolff, C.R. McIntyre, *Solid State Commun.* **71**, 355 (1989).

[18] B.E. Larson, *J. Appl. Phys.* **67**, 5240 (1990).

[19] Y. Shapira, T.Q. Vu, B.K. Lau, S. Foner, E.J. McNiff Jr., D. Heiman, C.L.H. Thieme, C.-M. Niu, R. Kershaw, K. Dwight, A. Wold, V. Bindilatti, *Solid State Commun.* **75**, 201 (1990).

[20] S. Isber, M. Averous, Y. Shapira, V. Bindilatti, A.N. Anisimov, N.F. Oliveira Jr., V.M. Orera, M. Demianiuk, to be published.

[21] T. Hoshina, *J. Phys. Soc. Jpn.* **21**, 1608 (1966).

[22] C. Testelin, A. Mauger, C. Rigaux, M. Guillot, A. Mycielski, *Solid State Commun.* **71**, 923 (1989); *Phys. Rev. B* **46**, 2193 (1992).

[23] M. Villeret, S. Rodriguez, E. Kartheuser, *Phys. Rev. B* **43**, 3443 (1991).

[24] T. Fries, Y. Shapira, A. Twardowski, E.J. McNiff Jr., T.Q. Vu, R. Kershaw, K. Dwight, A. Wold, *Phys. Rev. B,* in press.

[25] T.Q. Vu, *Solid State Commun.* **76**, 605 (1990); *Solid State Commun.* **81**, 583 (1992).

[26] D. Scalbert, M. Guillot, A. Mauger, J.A. Gaj, J. Cernogora, C. Benoit à la Guillaume, A. Mycielski, *Solid State Commun.* **76**, 977 (1990); C. Testelin, C. Rigaux, A. Mauger, D. Scalbert, C. Benoit à la Guillaume, A. Mycielski, M. Guillot, *J. Appl. Phys.* **70**, 6383 (1991).

[27] N.F. Oliveira Jr., S. Foner, Y. Shapira, T.B. Reed, *Phys. Rev. B* **5**, 2634 (1972).

[28] D. Kostyk, Y. Shapira, E.J. McNiff Jr., T.Q. Vu, A. Twardowski, to be published.

[29] J. Heremans, D.L. Partin, *Phys. Rev. B* **37**, 6311 (1988).